HHS Public Access

Author manuscript

Int J Radiat Oncol Biol Phys. Author manuscript; available in PMC 2020 March 01.

Published in final edited form as:

Int J Radiat Oncol Biol Phys. 2019 March 01; 103(3): 767–774. doi:10.1016/j.ijrobp.2018.10.030.

Rapid Multisite Remote Surface Dosimetry for Total Skin Electron Therapy: Scintillator Target Imaging

Irwin Tendler MEng[*], **Petr Brůža, PhD**[*], **Jacqueline Andreozzi, PhD**[*], **Michael Jermyn, PhD**[*], **Benjamin Williams, PhD**[*], **Lesley Jarvis, MD, PhD**[†,‡], **Brian Pogue, PhD**[†,‡], and **David Gladstone, ScD**[*,†,*,†,‡]

[*]Thayer School of Engineering, Geisel School of Medicine, Dartmouth College, Hanover, New Hampshire

[†]Department of Medicine, Geisel School of Medicine, Dartmouth College, Hanover, New Hampshire

[‡]Norris Cotton Cancer Center, Dartmouth-Hitchcock Medical Center, Lebanon, New Hampshire

Abstract

Purpose: The goal of this work is to produce a surface-dosimetry method capable of accurately and remotely measuring skin dose for patients undergoing total skin electron therapy (TSET) without the need for postexposure dosimeter processing. A rapid and wireless surface-dosimetry system was developed to improve clinical workflow. Scintillator-surface dosimetry was conducted on patients undergoing TSET by imaging scintillator targets with an intensified camera during TSET delivery.

Methods and Materials: Disc-shaped scintillator targets were attached to the skin surface of patients undergoing TSET and imaged with an intensified, time-gated, and linear accelerator—synchronized camera. Optically stimulated luminescence dosimeters (OSLDs) were placed directly adjacent to scintillators at several dosimetry sites to serve as an absolute dose reference. Real-time image-processing methods were used to produce background-subtracted intensity maps of Cherenkov and scintillation emission. Rapid conversion of scintillator-light output to dose was achieved by using a custom fitting algorithm and calibration factor. Surface doses measured by scintillators were compared with those from OSLDs.

Results: Absolute surface-dose measurements for 99 dosimetry sites were evaluated. According to paired OSLD estimates, scintillator dosimeters were able to report dose with <3% difference in 88 of 99 observed dosimetry sites and <5% difference in 98 of observed dosimetry sites. Fitting a linear regression to dose data reported by scintillator versus OSLD, per dosimetry site, yielded an $R^2 = 0.94$.

Reprint requests to: Lesley Jarvis, MD, PhD, Dartmouth-Hitchcock Medical Center, Section of Radiation Oncology, 1 Medical Center Dr, Lebanon, NH 03766. Tel: (603) 650-6600; lesley.a.jarvis@ hitchcock.org.

Conflict of interest: M.J. is an employee and B.P. is a president of DoseOptics LLC. P.B. is the principal investigator in SBIR subaward B02463 (prime award NCI R44CA199681, DoseOptics LLC).

Supplementary material for this article can be found at https://doi.org/10.1016/j.ijrobp.2018.10.030

Conclusions: Scintillators were able to report dose within <3% accuracy of OSLDs. Imaging of calibrated scintillator targets via an intensified, linear accelerator-synchronized camera provides rapid absolute surface-dosimetry measurements for patients treated with TSET. This technique has the potential to reduce the amount of time and effort necessary to conduct full-body dosimetry and can be adopted for use in any surface-dosimetry setting where the region of interest is observable throughout treatment.

Summary

Verifying radiation-field uniformity in total skin electron therapy is important to ensuring adequate and effective treatment administration. This clinical study presents a novel, scintillation-based, optical imaging technique for conducting surface dosimetry in patients undergoing total skin electron therapy. The system exceeded the ease of use of established dosimetry techniques at a similar level of accuracy.

Introduction

Total skin electron therapy

Total skin electron therapy (TSET) is an accepted and effective means for treating skin lymphoma; it has shown positive results in both palliative and chronic control of early-stage disease.[1–4] This treatment modality relies on administering a uniform electron field across the skin surface. Depending on institutional protocol, patients are positioned on either a rotary or a stationary stand at a source-to-surface distance (SSD) of 3 to 5 m. To ensure that all skin surfaces are exposed to the radiation beam, patients assume various stances by following methods such as the Stanford technique.

As per the recommendation of American Association of Physicists in Medicine - Task Group-121, it is important to verify dose across the skin surface to ensure adequate exposure and treatment efficacy.[5] Surface dosimetry plays a key role in quality assurance to ensure successful treat- ment.[6,7] Multisite dosimetry is frequently used throughout the course of treatment to verify patient skin-surface dose distributions.[8] Numerous commercial technologies exist for carrying out surface dosimetry for patients undergoing TSET; nevertheless, these methods have limitations in functionality and convenience.

Surface dosimetry: wireless dosimeters

Wireless devices provide dosimetric information without the need for data-transmission wires or cables. The active element, which is located either within a hard-plastic housing or wrapped cellophane, is directly attached to the skin to provide point dosimetry. The main drawback to these technologies is that measurement results are not available in real time. Current commercial wireless dosimeters require postexposure processing, or annealing. Common examples of remote dosimeters are alanine, thermoluminescent dosimeters (TLDs), and optically stimulated luminescent detectors (OSLDs). In the case of TLDs and alanine-based detectors, time-intensive postexposure annealing, on the order of 3 to 5 hours, is required for both readout and resetting.[9,10] OSLDs, on the other hand, do not require postexposure annealing; however, their use still necessitates allocation of resources to

postexposure readout; the OSLD reader must undergo daily quality assurance processes, and each OSLD must be processed one at a time.[11]

To obtain full-body surface dosimetry for a patient undergoing TSET using wireless dosimeters, numerous detectors must be placed across the body; the readout (and in some cases resetting) of each dosimeter imposes a time burden on staff. Because several dosimeters are placed onto the body simultaneously, the location of dosimeter placement must be rigorously tracked and recorded. This task is further complicated because these dosimeters are small and are changed in between TSET positions. For example, a given patient treatment using 3 TSET positions per day, with 7 dosimeters used for each position, requires that 21 unique dosimeter locations must be followed each time that surface dosimetry is conducted. Unfortunately, because human input inherently plays a key role in the use of these systems, a nontrivial chance of human error occurring exists.

Surface dosimetry: wired dosimeters

The active tips of wired dosimeters are placed on the patient's skin surface and connected by wire to a readout device for amplification and analysis. Examples of modern, live-readout dosimeters include metal-oxide semiconductor field-effect transistors, diodes, and scintillation-tip probes. To provide point dosimetry information, such as that from the wireless dosimeters discussed earlier, numerous live- readout detectors must be used to conduct full-body surface dosimetry. In practice, a clinical staff must keep track of dosimeter wires and ensure they are attached to the correct channels of the receiver; as with the currently available wireless dosimeter, this situation creates numerous opportunities for human error. In addition, attachment of numerous wires to the skin surface can prove to be both uncomfortable for the patient and cumbersome for the clinician (because wires must be removed and reattached when the patient is rotated).

Optical imaging methods

Previous work has shown that 2-dimensional scintillation dosimetry can be accomplished via optical imaging of flexible scintillating films.[12] However, from a clinical surface-dosimetry perspective, potential issues related to air gaps between the scintillating sheet and the skin surface are of concern. Optical imaging of Cherenkov emission from patients undergoing TSET has been previously described in the literature. Cherenkov emission can be directly related to absorbed dose in tissue; however, Cherenkov emission from human tissue is highly influenced by optical properties of the tissue. This phenomenon contributes to the heterogeneous distribution of Cherenkov intensity across the surface of a patient during TSET. Correcting Cherenkov intensity to account for optical properties of tissue is crucial for realizing accurate optical-surface dosimetry.[13–16]

Scintillation dosimetry

The currently available commercial technologies for surface dosimetry are cumbersome and require a substantial commitment of time and resources from clinical staff. We aim to create a system that avoids disadvantages associated with existing surface-dosimetry techniques while accurately reporting surface dose. Previous work demonstrated a novel whole-body surface dosimetry method capable of recovering dose from remote images of small

scintillator targets—thin plastic disks—in real time.[17] Light output from scintillator targets is energy independent.[18] Following this proof-of-concept study, we have evaluated the feasibility of using scintillator dosimeters to obtain remote, accurate, absolute dose measurements of the skin surface for patients undergoing TSET in a clinical setting.

Methods and Materials

Imaging setup

A linear accelerator (LINAC)—synchronized, time-gated, intensified camera (C-Dose Research; DoseOptics, Lebanon, NH) was positioned 4 m away from the patient to the side of the LINAC at a height of 1.13 m without shielding (Fig. 1A). A Canon (Canon, Tokyo, Japan) EF 24-mm f/1.4L II USM wide-angle lens was attached to the camera. The trigger mechanism of this camera system is described in Bruza et al[17] (2018). An optical data cable connected the camera to a computer outside of the LINAC vault.

The following real-time image-processing steps were performed during acquisition within the C-Dose software: (1) Background images underwent spatial median filtering, darkfield subtraction, and pulse normalization (division by the number of pulses in the background image). (2) Cher-enkov and scintillation data underwent spatial median filtering, temporal median filtering, darkfield subtraction, and background subtraction. This process subtracted the correct amount of background signal from the data image, the number of LINAC pulses with the differences in pulse duration, and exposure time between background and data considered. (3) Real-time background auto-equalization calculated a background-subtraction factor, accounting for overall intensity fluctuations between background and data (eg, temporal fluctuations in room lighting caused inherent to the alternating-current power supply). The subtraction factor is computed dynamically by obtaining a ratio of intensity between background (captured while no radiation is present) and subsequent Cherenkov frames (captured during beam on, includes background); the background is then subtracted out using that ratio. Every time a new Cherenkov frame is acquired, the ratio is checked with the most recent background frame and then used for subtraction. For the spatial and temporal median filters, a 5 × 5 pixel window size and a 5-image window size were used, respectively. Final outputs are 1600 × 1200 pixel intensity maps (.raw format) of background, Cherenkov, and scintillator emission. Video E1 (available online at https://doi.org/10.1016/j-%20ijrobp.2018.10.030) presents real-time cumulative images for a patient undergoing TSET in the anterior—posterior (AP) position.

Scintillators and multisite dosimetry

Disc-shaped (Ø 15 mm ×1 mm thick) scintillators were machined from EJ-212 plastic (Eljen Technologies, Sweetwater, TX) and painted along the edge and rear face with EJ-510 reflective paint. OSLDs were calibrated using recommendations from the manufacturer and the litera-ture.[19–21] Scintillator, OSLD, and TLD dosimeters are shown side by side for comparison in Figure 1A; these dosimeters are 1-, 2-, and 1-mm thick, respectively.

Scintillation dose-response calibration and phantom testing

Phantom experiments were used to produce a calibration factor converting scintillator output to dose. The 7 scintillators used for patient-surface dosimetry were attached to a flat-faced phantom. The phantom was positioned at a height of 1.2 m, SSD of 3 m, and 4 m from the camera. Each scintillator was paired with 2 OSLDs (nanoDot, Landauer Inc, Glenwood, IL) and 1 TLD (TLD-100 rods, Ø1 × 6 mm, ThermoFisher Scientific). The phantom was exposed to 100, 300, 600, 800, 1000, and 1200 MU high dose total skin electron (HDTSe) doses. A scintillation dose-response calibration factor was calculated by fitting a linear trendline to a plot of average dose reported by OSLD and TLD versus scintillator output.

Scintillator accuracy in reporting surface dose was verified using the same flat-faced phantom mentioned earlier. The scintillator dosimetry system, LINAC, and room-light conditions used in patient imaging were identical for this experiment (see the Patient dosimetry section for details). Each of the 7 scintillators was attached to the phantom and paired with 2 OSLDs. The phantom was positioned at a 3-m SSD in the center of the radiation field perpendicular to the incident beam and irradiated with a 6-MeV HDTSe beam for 303 MU. The camera was located adjacent to the gantry head 4 m away from the phantom at an angle of 15° to the phantom face; camera height was adjusted such that the phantom was located at the center of the field of view. The percent difference in surface dose reported by scintillator and OSLD was calculated.

Dose calculation

Absolute dose values were computed from the scintillator-light output using a custom image-processing algorithm (MATLAB, MathWorks, Natick, MA). A flat-field correction was applied to the images, and a region of interest (ROI) surrounding each scintillator target was selected (Fig. 1B, top right). A Gaussian-convolved-ellipse function was fit to each scintillator ROI per frame (Fig. 1B, bottom right). This function determines the x and y coordinates of the scintillator centroid, height and width of the ROI, maximum amplitude of fit, offset of fit, ellipse angle of rotation in radians, and Gaussian blur width per frame. The maximum amplitude of the fitted function was determined per frame and per scintillator (Fig. 1B, red arrow); the amplitude values per scintillator ROI were summed for all frames. The resulting summed amplitude value found for each scintillator ROI was converted to dose using a calibration factor.

Patient dosimetry

After receiving approval from the Dartmouth-Hitchcock Medical Center Internal Review Board, informed consent was obtained from all patients. A total of 3 patients were included in this study—2 were prescribed TSET for a treatment of mycosis fungoides and 1 for Kaposi sarcoma. To provide an absolute dose reference, OSLDs were placed directly adjacent to scintillators at each dosimetry site (Fig. 1A). Scintillators and OSLDs wrapped in clear cellophane were taped to the patient's skin on the upper arm, lower arm, chest, midsection, midthigh, midshin, and upper foot. The number of dosimetry sites was chosen based on earlier imaging and observations of where the dose was expected to vary significantly from umbilicus location. Patients were treated with 6-MeV HDTSe beam from a Trilogy (Varian Medical Systems, Palo Alto, CA) LINAC at a 3-m SSD (Fig. 1A). Patients

were positioned on a custom wooden stand adhering to the 6-position modified Stanford technique (AP, posterior—anterior [PA], right anterior oblique, left anterior oblique, right posterior oblique, and left posterior oblique). For each of these positions, treatments were delivered by upper and lower treatment fields using gantry angles of 289.5° and 250.5°, respectively. Patients were imaged under standard room-light conditions. During each dual-field TSET position treatment, a single scintillation video file was recorded at 7 frames per second.

Results

Patient imaging

Scintillation dosimetry data from 3 patients over the course of 16 TSET treatment days was analyzed. Patients were imaged 5, 7, 2, and 2 times in the AP, PA, right posterior oblique, and LPO positions, respectively. Image acquisition was dictated by patient compliance with TSET as well as availability of clinical and research resources. Images produced by the intensified camera displayed both Cherenkov and scintillation intensity maps. Figure 2 presents cumulative images corresponding to an entire set of 6 TSET positions for a given patient (Fig. 2 A–F); sample PA images are shown for the 2 other patients included in this study (Fig. 2 G–H). Surface dosimetry was not conducted during the anterior oblique or left anterior oblique positions because of patient fatigue (these positions are last in each corresponding TSET treatment sequence). The images show a nonuniform Cherenkov intensity across the body as well as scintillation signal in the form of bright dots at various anatomic sites.

Calibration for dose conversion: phantom data

TLDs were used in conjunction with OSLDs to provide a secondary surface-dose verification method during calibration experiments; however, only OSLDs were used for in vivo measurements because of ease of use. Agreement between OSLDs and TLDs was 3% ± 1%. A calibration plot of summed scintillator-fit amplitude versus average dose reported by OSLD and TLD was used to convert scintillator output to surface dose (Fig. 3A). Error bars represent standard deviation (SD) in dose measured by reference dosimeters (TLD and OSLD) and scintillators; increases in SD at higher doses for reference dosimeters are expected and disclosed by the manufacturer.[22,23] Fluctuation in scintillator SD can be attributed to the low number of scintillator discs used; repeated tests with a larger sample size of scintillator dosimeters (n = 29) showed that scintillator SD was 1 ± 0.1 cGy consistently across all administered doses. The linear fit in Figure 3A resulted in an R^2 = 0.99. Thus, a linearcalibration factor for converting summed-fit amplitude per scintillator to dose (cGy) was generated and used for all scintillator dosimeters in this study.

Scintillation dosimetry accuracy

The accuracy of scintillator dosimeters was evaluated using phantom testing; the average percent difference between scintillators and OSLDs in measuring surface dose was 0.6% ± 0.2%. For patient imaging, each dosimetry site was considered an independent measurement of surface dose reported by scintillator versus OSLD; neither TSET nor anatomic position associated with a given dosimetry site were considered in analysis. For a

comparison to the treatment plan, dose at the umbilicus dosimetry site was tracked for a patient throughout a full cycle of 6 TSET positions; given a treatment plan of 200 cGy, total dose at this site was measured by scintillator and OSLD to be 183.9 and 182.2 cGy, respectively. The accuracy of scintillation dosimeters to measure surface dose for patients undergoing TSET was evaluated for a total of 99 dosimetry sites. Each dosimetry site featured a scintillator and OSLD placed directly adjacent to one another. The specific breakdown of dosimetry-site locations per patient is shown in Table 1. Percent difference between surface dose determined by scintillation dosimeters compared with OSLDs was found to be <5% in 98 of 99 and <3% in 88 of 99 dosimetry sites (Fig. 3B)—the maximum difference, 5.4%, was observed at the upper arm of a PA position. Furthermore, it was found that fitting a linear trend line to a plot of scintillator versus OSLD dose per dosimetry site for all patients resulted in a fit coefficient of determination (R^2) = 0.94 and root mean square error of 1.1 cGy. Ninety-seven of 99 dosimeter comparisons fall within a ±95% confidence interval (Fig. 3C); the R^2 and root mean square error of the fit between dose reported by scintillator compared with OSLD per patient ranged from 0.92 to 0.94 and 0.9 to 1.2, respectively.

Discussion

This scintillator-based surface-dosimetry system was capable of reporting dose with a relative accuracy comparable to OSLD dosimeters in a real-world clinical scenario. In constructing the scintillator dosimeter imaging system, previously described angular and distance dependencies were considered.[18] To minimize these effects, the design of this system was optimized for TSET imaging; camera settings and the dosimeter type, size, and shape were dictated by clinical requirements of this treatment modality. This system can report surface dose independent of camera- scintillator or incident radiation-scintillator angles within the range of 0° to 55°. Imaging of scintillator targets can be conducted at angles outside of this range as long as the face of the scintillator is in view of the camera; however, correction for angular dependence must be implemented. In cases of angles >80°, usability of this dosimetry system becomes limited.

Scintillator dosimetry is also independent of change in camera-scintillator distance within 1.5 m. Given that patients are instructed to stand still during treatment and scintillators are attached to the skin such that they face toward the camera, surface-dose readout could be accomplished without correction for angle or distance. In conducting scintillator dosimetry, no system-related testing was completed before each treatment, but the linearity of signal with dose was directly derived from the types of scintillators attached to the stand, which were never moved.

Reference scintillators (of various sizes) were attached to the TSET patient stand (Fig. 1A); their emission was captured within each patient treatment image frame (Fig. 1B) so that multiple reference measurements were automatically obtained. Reference scintillator output collected during calibration of the system was used as a baseline to continually provide information regarding stability and performance of the scintillator dosimetry system. Specifically, the camera was checked for damage every day when imaging the beam via monitoring of the reference scintillator light emission on the stand. During this study, the

camera was stable within 2% ± 1% (measured using reference scintillators), and on a monthly basis there is expected to be a quality assurance calibration check. It is likely that this camera, as with all Complimentary Metal- Oxide-Semiconductor technology, will fail at a certain radiation dose, but this issue has not been observed yet. Daily checking continues to ensure that signal intensities are comparable between imaging sessions.

Optical imaging of Cherenkov emission from patients undergoing TSET has been previously described in the literature; Cherenkov emission is proportional to absorbed dose in tissue. However, as shown in both previous work and this study, it is highly influenced by optical properties[14–16] in tissues (see Fig. 1B and 2). Correcting Cher-enkov intensity to account for optical properties in tissues is required but not yet developed, to enable optical surface dosimetry directly from patient skin. Scintillation produced by the unique dosimeters described in this article is emitted independently of optical properties in tissues—dosimeter locations were chosen to best exemplify the distribution of Cherenkov across a range of body-surface locations vertically. Painting the rear face and edge of the scintillator disc with reflective coating prevented contamination of scintillator signal by Cherenkov light produced in tissue underlying the scintillator.

By analyzing the dose reported by OSLD versus scintillator at each dosimetry site independently of patient body type, body location, or TSET position, we have shown that scintillation dosimetry has the potential to be a robust tool for multisite measurement of surface dose during TSET. In addition, this system could be adapted for use in the rotational TSET treatment geometry by simultaneously acquiring images using multiple cameras to result in a 360° field of view. Complementary orthovoltage or electron fields are commonly used to provide irradiation to parts of the body shielded from the TSET technique, such as the soles of the feet or the groin. Because these sites are not visible and the scintillators do not store absorbed dose signal, this dosimetry technique is not applicable to sites needing a radiation boost by use of complementary fields. The current design of this system can be adopted for use in real-time surface dosimetry—optimization of the scintillator output to the dose-conversion algorithm can be made to enable more rapid dose measurements. For example, every 5 frames would be summed, scintillator output for this period will be converted to dose, and an on-screen dose-counter per scintillator will be updated. Furthermore, because image acquisition is gated to, and triggered by, LINAC pulses, the scintillator dosimetry system can be modified such that an alert is displayed (or if desired, treatment terminated) when the acquisition rate drops below a defined threshold.

Conclusions

Skin-surface dosimetry was conducted in patients being treated with TSET by converting light emission from scintillators to dose. Scintillator dosimeter light output linearly increases with dose, has a fluence approximately 100 times more intense than Cherenkov emission from tissue, can be remotely detected in ambient room-light settings, and can provide rapid surface-dose data. Dose reported by scintillators corresponds to that measured by OSLDs with a discrepancy of <3% in 88 of 99 cases. Compared with current surface-dosimetry techniques, this system has the potential to reduce the amount of time and resources necessary to perform multisite surface dosimetry for patients undergoing TSET. The

resulting dose images can be automatically stored in the medical record, avoiding all sources of errors accompanied with detector manipulation, readout, manual dose-value recording, and even patient misidentification. Customizing dosimeters for medical use will further aid in improving TSET-associated surface dosimetry workflow.

Supplementary Material

Refer to Web version on PubMed Central for supplementary material.

Acknowledgments

This work was sponsored by National Institutes of Health grants R44 CA199836, R01 EB023909, and P30 CA023106.

References

1. Evans MDC, Hudon C, Podgorsak EB, et al. Institutionalexperiencewitha rotational total skin electron irradiation (RTSEI) technique—A three decade review (1981–2012). Rep Pract Oncol Radiother 2013;19:120–134. [PubMed: 24936331]
2. Heumann TR, Esiashvili N, Parker S, et al. Total skin electron therapy for cutaneous T-cell lymphoma using a modern dual-field rotational technique. Int J Radiat Oncol Biol Phys 2015;92:183–191. [PubMed: 25670538]
3. Hauswald H, Zwicker F, Rochet N, et al. Total skin electron beam therapy as palliative treatment for cutaneous manifestations of advanced, therapy-refractory cutaneous lymphoma and leukemia. Radiat Oncology 2012;7:118.
4. Reynard EP, Evans MDC, Devic S, et al. Rotational total skin electron irradiation with a linear accelerator. JAppl ClinMed Phys 2008;9:123–134.
5. Hensley FW, Major G, Edel C, et al. Technical and dosimetric aspects of the total skin electron beam technique implemented at Heidelberg University Hospital. Rep Pract Oncol Radiother 2013;19:135–143. [PubMed: 24936332]
6. Desai KR, Pezner RD, Lipsett JA, et al. Total skin electron irradiation for mycosis fungoides: Relationship between acute toxicities and measured dose at different anatomic sites. Int J Radiat Oncol Biol Phys 1988;15:641–645. [PubMed: 3138216]
7. Kumar PP, Henschke UK, Nibhanupudy JR. Problems and solutions in achieving uniform dose distribution in superficial total body electron therapy. J Natl Med Assoc 1977;69:645–647. [PubMed: 143541]
8. Antolak JA, Cundiff JH, Ha CS. Utilization of thermoluminescent dosimetry in total skin electron beam radiotherapy of mycosis fun-goides. Int J Radiat Oncol Biol Phys 1998;40:101–108. [PubMed: 9422564]
9. Tsai WC, Jiang SH. A study on annealing technique for Lif: Mg,Cu,P thermoluminescent dosimeter. Radiat Meas 2011;46: 1595–1597.
10. Heydari MZ, Malinen E, Hole EO, et al. Alanine radicals. 2. The composite polycrystalline alanine EPR spectrum studied by ENDOR, thermal annealing, and spectrum simulations. J Phys Chem A 2002; 106:8971–8977.
11. Pradhan AS, Lee JI, Kim JL. Recent developments of optically stimulated luminescence materials and techniques for radiation dosimetry and clinical applications. J Med Phys 2008;33:85–99. [PubMed: 19893698]
12. Jenkins CH, Naczynski DJ, Yu S-JS, et al. Monitoring external beam radiotherapy using real-time beam visualization. Med Phys 2015;42: 5–13. [PubMed: 25563243]
13. Andreozzi JM, Zhang R, Gladstone DJ, et al. Cherenkov imaging method for rapid optimization of clinical treatment geometry in total skin electron beam therapy. Med Phys 2016;43:993–1002. [PubMed: 26843259]

14. Xie Y, Petroccia H, Maity A, et al. Cherenkov imaging for Total Skin Electron Therapy (TSET). SPIE Proceedings In: Molecular-Guided Surgery: Molecules, Devices, and Applications IV, 10478. International Society for Optics and Photonics; 2018 p. 1047816.
15. Glaser AK, Zhang R, Gladstone DJ, et al. Optical dosimetry of radiotherapy beams using Cherenkov radiation: the relationship between light emission and dose. Phys Med Biol 2014;59:3789. [PubMed: 24938928]
16. Andreozzi JM, Bruza P, Tendler II, et al. Improving treatment geometries in total skin electron therapy: Experimental investigation of linac angles and floor scatter dose contributions using Cherenkov imaging. Med Phys 2018;45:2639–2646. [PubMed: 29663425]
17. Bruza P, Gollub S, Andreozzi J, et al. Time-gated scintillator imaging for real-time optical surface dosimetry in total skin electron therapy. Phys Med Biol 2018;63;095009.
18. Beaulieu L, Goulet M, Archambault L, et al. Current status of scintillation dosimetry for megavoltage beams. J Phys: Conf Ser 2013; 444:012013.
19. Souri S, Ahmed Y, Cao Y, et al. SU-E-T-638: Evaluation and comparison of Landauer Microstar (OSLD) readers. Med Phys 2016;41: 374–375.
20. Kry S The clinical use of OSLD. AAPM; 2015 Available at: http://amos3.aapm.org/abstracts/pdf/97-25841-352470-109886-71671192.pdf.
21. Yahnke CJ. Calibrating the microStar, Rev. Landauer Inc; 2009 Available at: https://pdfs.semanticscholar.org/d29d/e4a28e2e10314d20b92fc4ac75e88a3a1125.pdf.
22. Landauer. nanoDot Dosimeter - Patient Monitoring Solutions, Rev. Landauer Inc; 2017 Available at: https://www.landauer.com/sites/default/files/product-specification-file/nanoDot_0.pdf.
23. Aguirre J, Alvarez P, Ibbott G, et al. Analysis of uncertainties for the RPC remote dosimetry using optically stimulated light dosimetry. Med Phys 2011;38:1118.

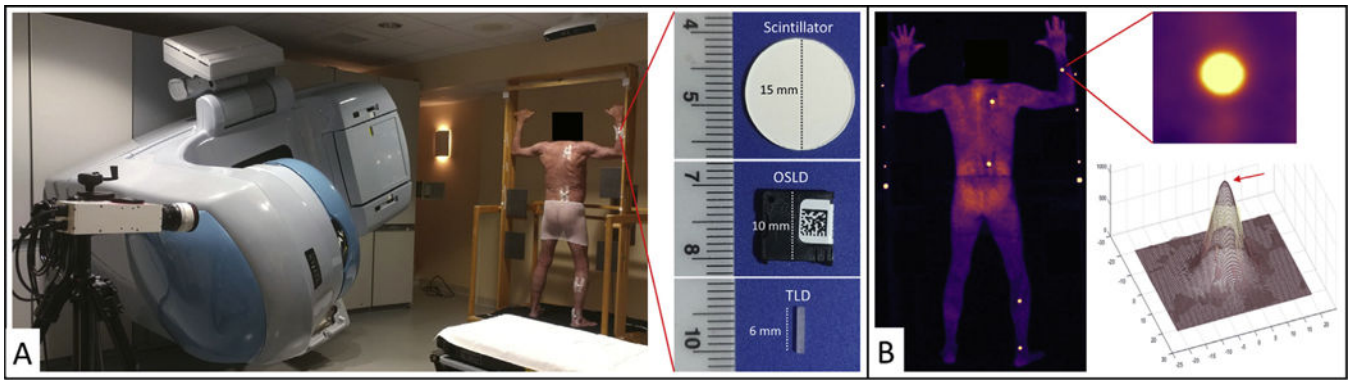

Fig. 1.

Room setup, dosimeter application, and comparison of image processing. (A) Photograph of a patient on a custom total skin electron therapy stand, linear accelerator, and intensified camera. Zoomed-in view of a dosimeter packet attached to a patient provides a close-up perspective on the face of a scintillator, optically stimulated luminescence dosimeter, and thermoluminescent dosimeter. Width dimensions are provided in mm. (B) Background-subtracted cumulative image of the patient from panel A. Zoomed-in view provides region of interest of scintillator used in image processing (upper right) and ellipse-convolved Gaussian fit to a single frame of the scintillation video. The red arrow points to the maximum amplitude value. (A color version of this figure is available at https://doi.org/10.1016/jijrobp.2018.10.030.)

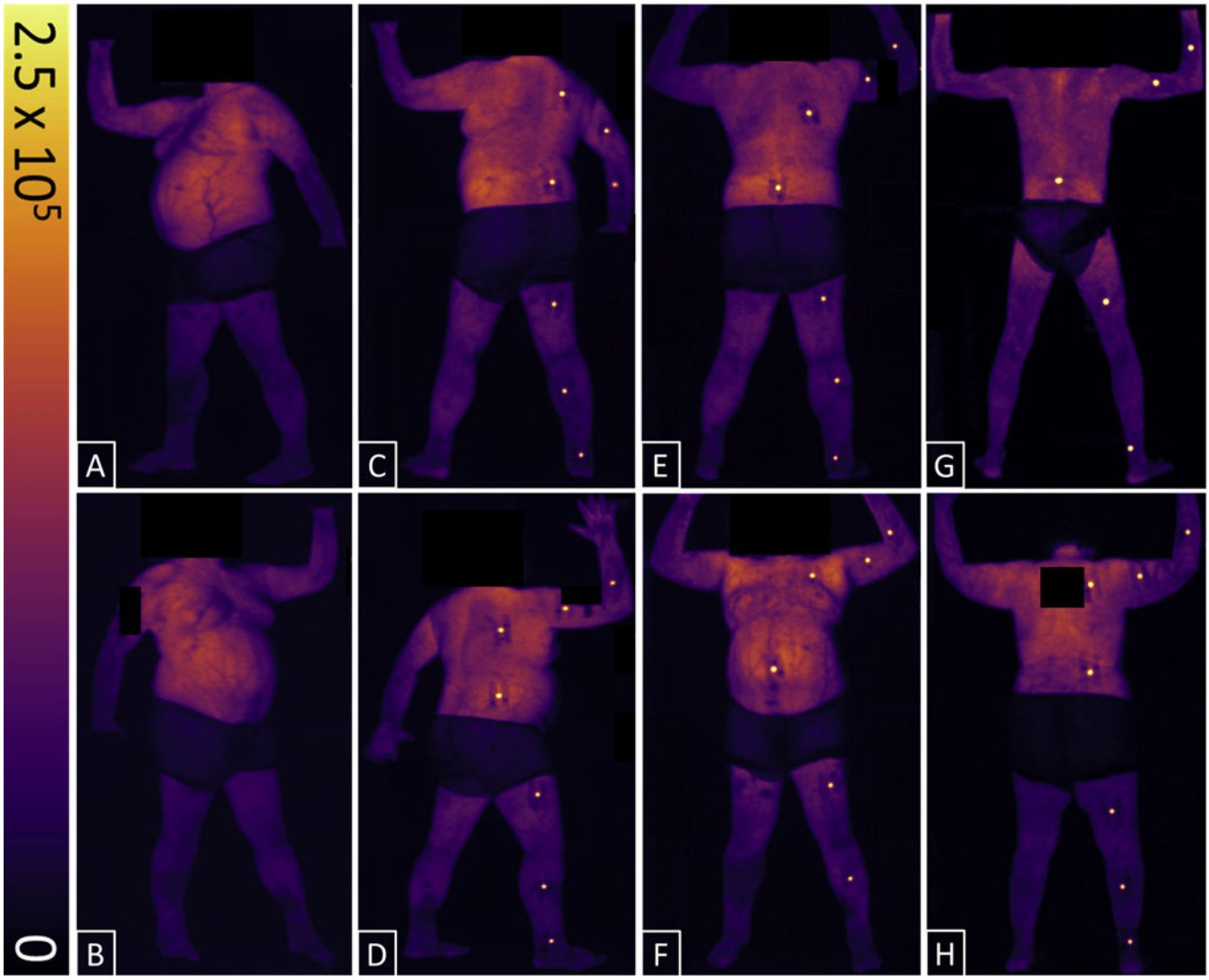

Fig. 2.

Cumulative, background-subtracted, Cherenkov, and scintillation-intensity maps for patients undergoing total skin electron therapy. All 6 total skin electron therapy positions are shown for 1 patient: left anterior oblique (A), right anterior oblique (B), left posterior oblique (C), right posterior oblique (D), posterior-anterior (E), and anterior-posterior (F). Sample images from the 2 other patients in the posterior—anterior position are shown in G and H. Color-intensity scale is in digital units. Dark areas around the midsection of patients are caused by cloth shorts; all identifying features have been anonymized.

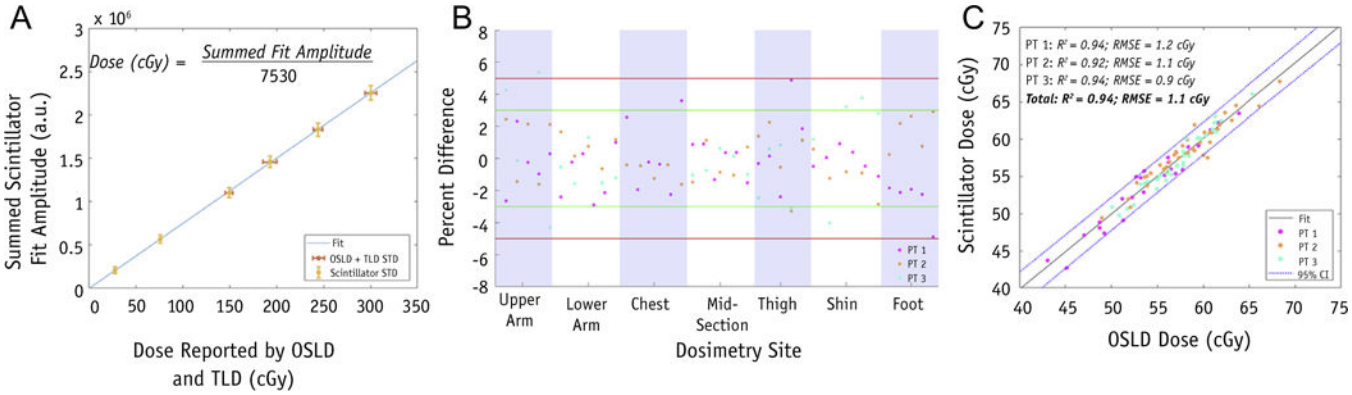

Fig. 3.

Plots for calibration, percent difference, and scintillator versus OSLD dose measurements. (A) Summed-fit amplitudes (a.u.) averaged for all scintillators and corresponding dose reported by averaging OSLD (cGy), standard error for OSLD + TLD, and scintillators shown in red and yellow, respectively. The equation for obtaining the calibration factor is provided. (B) Percent difference in dose reported by scintillator and OSL dosimeters per dosimetry site for all patients; ±5% and ±3% shown in red and green, respectively. (C) Dose measured by scintillator versus OSLD per dosimetry site; linear trendline and 95% confidence interval are plotted. R^2 and root mean square error are shown for both individual patients and the entire cohort. *Abbreviations:* a.u. = summed-fit amplitudes; CI = confidence interval; OSLD = optically stimulated luminescence dosimeters; PT = patient; RMSE = root mean square error; TLD = thermoluminescent dosimeters. (A color version of this figure is available at https://doi.org/10.1016/j.ijrobp.2018.10.030.)

Table 1

Dosimetry-site breakdown

Patient no.	TSET positions	Dosimetry-site locations	Total no. of sites	<5% difference	<3% difference
1	3 AP	3 UA + 3 LA + 3 MID + 3 MT + 3 MS	15	14/15	10/15
	2 AP	2 UA + 2 LA + 2 MID + 2 MT + 2 MS	10	10/10	8/10
	1 AP	0 UA + 1 LA + 1C + 1 MID + 1 MT + 1 MS + 0 UF	5	5/5	5/5
	2 AP	2 UA + 2 LA + 2 C + 2 MID + 1 MT + 2 MS + 2 UF	13	13/13	13/13
2	1 LPO	1 UA + 1 LA + 1C + 1 MID + 1 MT + 1 MS + 1 UF	7	7/7	6/7
	2 RPO	2 UA + 2 LA + 2 C + 2 MID + 2 MT + 2 MS + 2 UF	14	14/14	12/14
	1 AP	1 UA + 1 LA + 1C + 1 MID + 1 MT + 1 MS + 1 UF	7	7/7	6/7
3	3 PA	3 UA + 3 LA + 3 C + 3 MID + 3 MT + 3 MS + 3 UF	21	21/21	21/21
	1 RPO	1 UA + 1 LA + 1C + 1 MID + 1 MT + 1 MS + 1 UF	7	7/7	7/7
Total	5 AP + 7 PA + 2 LPO + 2 RPO	15 UA + 16 LA + 11 C + 16 MID + 15 MT + 16 MS + 15 UF	99	98/99	88/99

Abbreviations: AP = anterior-posterior; C = chest; LA = lower arm; LPO = left posterior oblique; MID = midsection; MS = midshin; MT = midthigh; PA = posterior-anterior; RPO = right posterior oblique; TSET = total skin electron therapy; UA = upper arm; UF = upper foot.

The following are provided for each patient: type and number of TSET positions imaged, location and number of all dosimetry sites, total number of sites analyzed, and percent difference (<3% and <5%) in surface dose measured by scintillator and optically stimulated luminescence dosimeters per TSET position.